

Locality and topology with fat link overlap actions

Tamás G. Kovács

*NIC/DESY, Platanenallee 6
D-15738 Zeuthen, Germany
e-mail: kovacs@ifh.de*

and

*Department of Theoretical Physics¹
University of Pécs
H-7624 Pécs, Ifjúság útja 6.*

Abstract

We study the locality and topological properties of fat link clover overlap (FCO) actions. We find that a small amount of fattening (2-4 steps of APE or 1 step of HYP) already results in greatly improved properties compared to the Wilson overlap (WO). We present a detailed study of the localisation of the FCO and its connection to the density of low modes of $A^\dagger A$. In contrast to the Wilson overlap, on quenched gauge backgrounds we do not find any dependence of the localization of the FCO on the gauge coupling. This suggests that the FCO remains local in the continuum limit. The FCO also faithfully reproduces the zero mode wave functions of typical lattice instantons, not like the Wilson overlap. After a general discussion of different lattice definitions of the topological charge we also show that the FCO together with the Boulder charge are likely to satisfy the index theorem in the continuum limit. Finally, we present a high statistics computation of the quenched topological susceptibility with the FCO action.

1 Introduction

In recent years one of the most important technical and conceptual advances in the lattice discretisation of QCD has been the discovery and practical implementation of chirally symmetric lattice fermion actions. While in the continuum limit chiral symmetry is expected to be recovered in any lattice discretisation of fermions, the new formulation guarantees that it already holds exactly at non-zero lattice spacings. This

¹Address after October 1, 2002.

has important practical consequences opening new possibilities in the study of QCD with light quarks.

By now, there are several different implementations of chirally symmetric lattice fermions (see e.g. Ref. [1]), but being relatively new, the properties of these implementations have not yet been fully explored. Certainly many questions are still to be answered before chiral fermions can reach their full potential. In particular, speed, scaling properties and locality are just some of the issues that clearly play an important role in this context and have to be optimized before chiral fermions can make their way into realistic full (unquenched) QCD simulations.

In the present paper we propose to study a simple variant of one of the formulations of chiral fermions, namely the overlap [2]. The basic overlap construction starts with any “reasonable” Dirac operator, D_0 , that is used as a “kernel” in the overlap construction. The overlap operator is defined in terms of D_0 by the formula

$$D_{\text{ov}} = 1 - A [A^\dagger A]^{-\frac{1}{2}}, \quad A = 1 + s - D_0, \quad (1)$$

where s is a real parameter. In the original overlap construction D_0 was the Wilson lattice Dirac operator. It is by now clear, however, that properties of the overlap depend strongly on what operator is used for D_0 [4]-[6]. In the construction we propose here, D_0 is the clover improved Dirac operator with the tree-level value of $c_{\text{sw}} = 1.0$ and smeared fat gauge links [3]. This construction is neither particularly imaginative, nor is it new. In particular, fattened gauge links are used in more complicated overlap kernels [4, 5] and the type of fat link clover overlap (FCO) we propose here has already been used to estimate the quark-mass dependence of the unquenched topological susceptibility [7]. The authors of Ref. [8] argue that the evaluation of the FCO—although a slightly different version thereof—is roughly two times faster than the Wilson overlap, due to the better condition number of $A^\dagger A$.

The reason why we propose to study some properties of the FCO in more detail is that it might represent an optimal compromise between much more complicated choices of D_0 and the Wilson overlap. In the present paper we shall explicitly demonstrate that the FCO action has the following advantages compared to the Wilson Overlap (WO).

- Already after a very small amount of fattening, lattice configurations are smooth enough that the parameter s does not have to be tuned, it can be set to zero independently of the gauge coupling. This feature also makes it possible to check that the localisation range of D_{ov} does not change as the gauge coupling is varied.
- The operator $A^\dagger A$ is much better conditioned which translates into savings of a factor of 2–5 in computing time when evaluating its inverse square root.
- In contrast to the WO [10], the FCO precisely reproduces the continuum wave function of quark zero modes in the background of smooth instantons down to an instanton size of one lattice spacing.

The downside is, purists might object, that using fat gauge links might affect short distance properties. This however is not a real problem, since very little fattening turns out to be enough to ensure the above listed good properties. We shall also explicitly check how non-local the APE smearing is and find that the needed smearing is actually more localized than the overlap itself. Even better, one step of “HYP” smearing [13], a smearing that stays within a hypercube, is already enough to guarantee the above listed good properties.

In Section 2 we test the locality of both the APE smearing and the overlap operator. We find that the (exponential) localisation range of the FCO is essentially independent of the gauge coupling of the background gauge fields in the range of (Wilson) $5.7 \leq \beta \leq 6.0$, where we tested it. The most important consequence of this is that the FCO action is very likely to remain local in the continuum limit. In fact, at these gauge couplings the localisation range of the FCO turns out to be somewhat smaller than that obtained for the WO after optimizing the parameter s .

We also discuss the possible role of small eigenvalues of $A^\dagger A$ in the locality properties of the overlap. We find that although the spectral density of $A^\dagger A$ is divergent at zero, small eigenmodes occur with a finite probability, decreasing towards the continuum limit. They seem to be related to gauge field defects living on the scale of the cut-off and the localisation of the corresponding eigenmodes stays constant in lattice units as the continuum limit is approached. Therefore, they are very unlikely to affect the locality of the overlap in the continuum limit.

In Section 3 we study the topological properties of quenched gauge fields with the FCO operator. We demonstrate that—unlike the Wilson overlap—the FCO reproduces continuum instanton zero mode wave functions down to lattice instanton sizes of $\rho/a \approx 1 - 2$. We also discuss the criteria for a fermionic and a gauge field definition of the topological charge to satisfy the index theorem in the continuum limit. We find that the FCO Dirac operator and the Boulder charge satisfy these criteria. Finally we present a high statistics computation of the quenched topological susceptibility using both definitions of the charge.

2 Locality

Locality is a crucial property of lattice actions since it guarantees that physics in the continuum limit is independent of the details of the discretisation (universality). Most of the conventional lattice QCD actions, both fermionic and gauge actions, are ultralocal. This means that they connect only degrees of freedom up to a finite distance measured in lattice units. It has been proved that there is no chirally symmetric lattice fermion action that is ultralocal [11], therefore if we insist on chiral symmetry, we have to settle with a weaker form of locality. We demand only that the matrix elements of the operator should fall off exponentially with the distance measured in lattice units and that this exponent should be non-zero in the continuum limit. This weaker form of locality is still enough for universality. In the present section we study the locality

of the two ingredients of our FCO action, the smeared gauge links and the fermion action itself.

2.1 Smearing

The smearing that we use on the gauge links entering the fermion operator consists of two steps. First, each link is replaced with a linear combination of itself and the six shortest staples around it, as

$$U_\mu(x) \longrightarrow U'_\mu(x) = (1 - c)U_\mu(x) + \frac{c}{6} \sum_{\nu \neq \mu} \left(S_\mu^{(\nu)}(x) + S_\mu^{(-\nu)}(x) \right), \quad (2)$$

where $S_\mu^{(\nu)}(x)$ is the product of gauge links along the path $(x, x + \hat{\nu}, x + \hat{\nu} + \hat{\mu}, x + \hat{\mu})$, the staple and c is a real parameter. Since a linear combination of $SU(3)$ elements is in general not an element of the group, in the second step $U'_\mu(x)$ is projected back to the gauge group by minimizing $\text{tr} U_\mu'^{\dagger}(x) \mathcal{P}(U'_\mu(x))$ for all possible $\mathcal{P}(U'_\mu(x)) \in SU(3)$.

One sweep of this procedure through the whole lattice will be referred to as one step of APE smearing. In the course of a sweep the new smeared links are always constructed from the original ones without immediate replacement. The original gauge links are replaced with the new smeared ones only after a full sweep through the lattice has been completed. Therefore, the procedure is independent of the order in which the gauge links are smeared and it is also strictly ultralocal.

Since any finite number of APE smearing steps is ultralocal, from a conceptual point of view operators constructed from smeared links are as good as any other local operator, as long as the number of smearing steps is kept constant in the continuum limit. There is, however, a more practical issue. In actual simulations, it is desirable to keep the “size” of operators much smaller than the inverse mass of the heaviest physical particle in the system, otherwise strong scaling violations can be expected. For this reason, in the present section we check how the locality of smearing depends on the number of smearing steps and the smearing coefficient, c .

The simplest way of doing that is by monitoring how a local disturbance in the gauge field is propagated into gauge invariant quantities measured at a distance from the disturbance. We choose the most local disturbance, a random change of a single gauge link and the simplest gauge invariant observable, the plaquette. After randomly flipping a single gauge link, we compute the modulus of the difference between each smeared plaquette of the original and the changed configuration. Let us denote this quantity, averaged over all 24 plaquettes at site x , by $\delta p(x)$. We are interested in how $\delta p(x)$ changes with the distance from the flipped link at $x = 0$. Therefore, the quantity we look at is $\overline{\delta p}(r)$, the average of $\delta p(x)$ over spherical shells of radius $r = |x|$, normalized such that $\overline{\delta p}(0) = 1$.

In Fig. 1 $\overline{\delta p}(r)$ versus r is shown, averaged over a set of 50 quenched Wilson $\beta = 5.94$ 12^4 lattice configurations. In this computation c was (arbitrarily) set to 0.45 and the number of smearing steps shown are 2,4,6,10,16 and 24. The important feature we have to notice here is that for moderate smearing (about $n < 10$), $\overline{\delta p}(r)$ decays faster

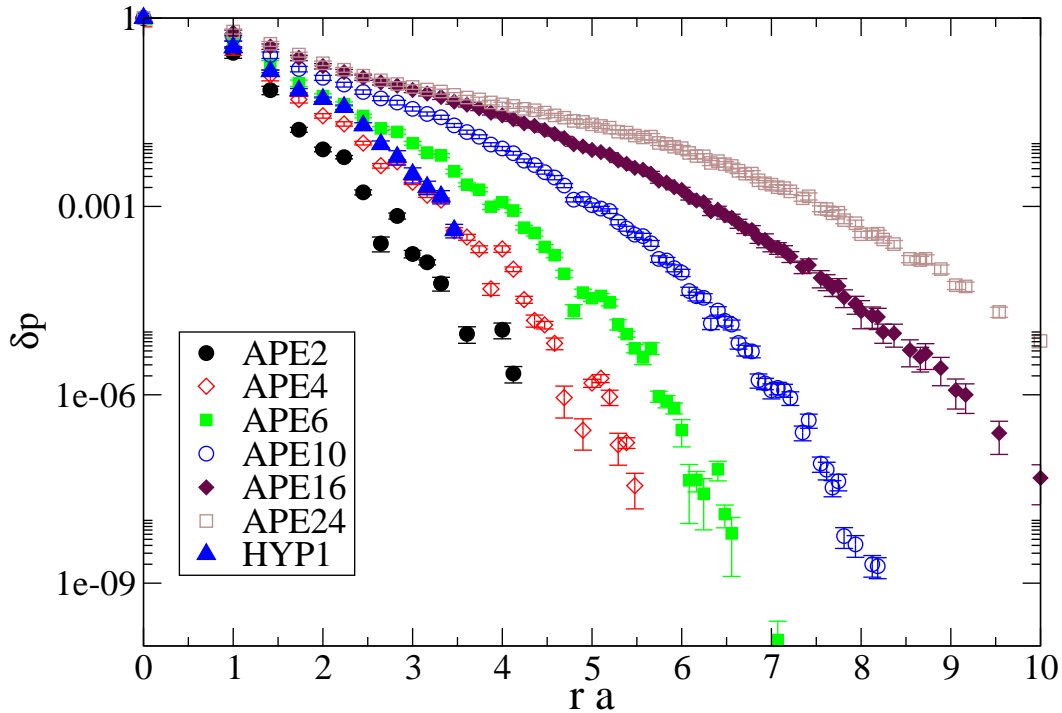


Figure 1: The range of APE smearing as measured by the change of the average smeared plaquette ($\overline{\delta p}$) due to flipping a single link. ra is the distance from the flipped link and the curves correspond to 2,4,6,10,16 and 24 (from left to right) steps of APE smearing with $c = 0.45$, and 1 step of HYP smearing (triangles).

than exponentially over the whole range where it is non-zero. The starting exponents, that were fit in the range $1 \leq r \leq 3$ vary from 4.0 to 1.3 for 2 and 10 steps of smearing respectively. Notice that the actual decay rate of $\overline{\delta p}(r)$ for $r \geq 3$ is much faster than that.

If more than about 10 smearing steps are applied, the function $\overline{\delta p}(r)$ slowly starts to develop a “shoulder” that gradually extends to larger distances. In other words this means that for more than 10 smearing steps the logarithmic derivative of $\overline{\delta p}(r)$ is not monotonous; the initial short distance exponential decay rate slows down at medium distances of $r \approx 3 - 5$ before accelerating again above that.

From this behaviour we can conclude that for most physical quantities, operators built of 2-4-smearred links should be quite safe, and even as much as 10 steps of smearing might not be too severe. Going beyond this point, however, smearing will start to affect medium distance properties and might have an adverse effect on spectral quantities.

For comparison we also plotted $\overline{\delta p}(r)$ for one step of HYP smearing that is strictly localized within a hypercube (triangles in Fig. 1). Regarding the properties of the smeared configurations, HYP1 is roughly equivalent to APE4. The initial fall-off of $\overline{\delta p}(r)_{\text{HYP1}}$ is slightly slower than that of APE4, however, $\overline{\delta p}(r)_{\text{HYP1}}$ vanishes for $ra \geq$

3.5.

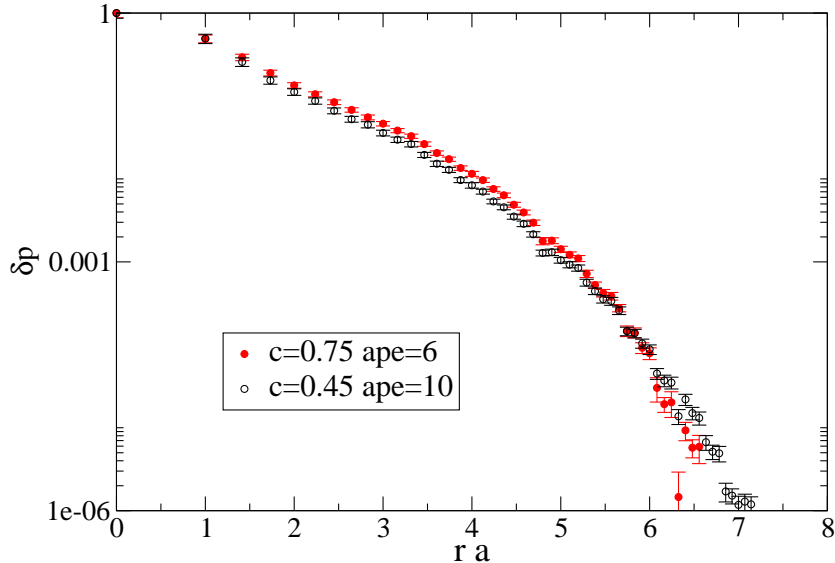


Figure 2: The same as Fig. 1 but here 6 steps of $c = 0.75$ smearing is compared to 10 steps of $c = 0.45$ APE smearing.

We also briefly experimented with APE smearing coefficients other than $c = 0.45$ and confirmed the previously established rule of thumb that the extent of APE smearing can be adequately characterized with c times the number of smearing steps². To illustrate this point, in Fig. 2 we compare the behaviour of $\overline{\delta p}(r)$ obtained with 10 steps of $c = 0.45$ and 6 steps of $c = 0.75$ APE smearing.

2.2 The fat link clover overlap

We now turn to testing the locality of the overlap operator itself. The simplest way to measure how its matrix elements fall-off with the distance is to create a delta source $\psi_k(x) = \delta(x)\delta_{kj}$ (k and j refer to Dirac and colour indices) and compute how $\|D_{ov}\psi(x)\|$ decays with the distance from the source.

In the only available detailed study of the locality of the Wilson overlap, the so called “taxi driver distance”, the sum of the moduli of the coordinate differences $r = \sum_{\mu} |x_{\mu}|$ was used and the function

$$f(r) = \max \left\{ \|D_{ov}\psi(x)\| : \sum_{\mu} |x_{\mu}| = r \right\} \quad (3)$$

was computed [9]. To be able to compare our results to those of Ref. [9], we first also compute this quantity for the FCO action.

²More precisely, this is true only as long as the smearing coefficient c is not bigger than its critical value of 0.75, which will always be the case here.

Before presenting our results, however, we have to briefly discuss how we choose the arbitrary parameter s in the overlap construction. If the Wilson action is used, the parameter s has to be optimized. Roughly speaking, s is an arbitrary “cut” that controls whether a given real eigenvalue of the Wilson operator between the physical modes and the doublers will become a low physical mode or a doubler of the resulting overlap. It is clearly advantageous, both from the practical and the conceptual point of view, to set s in a way to minimize the number of small eigenvalues of $A^\dagger A$. According to Ref. [9], e.g. at Wilson $\beta = 6.0$ the exponent governing the decay of $f(r)$ can vary between 0.28 and 0.49 as s changes from 0.0 to 0.4. In the continuum limit, the optimal value of s is expected to go to zero.

Since the localisation range of D_{ov} depends strongly on s , it is not an easy task to verify numerically that D_{ov} remains local in the continuum, i.e. that the exponent goes to a non-zero constant. To this end, one would need to compute the optimal exponent at every value of β and verify the statement for that. While the numerical results of Ref. [9] are encouraging in this respect, such a complete study was not undertaken there. Moreover, it is not guaranteed that the localization and the density of small eigenvalues of $A^\dagger A$ are optimal at the same s .

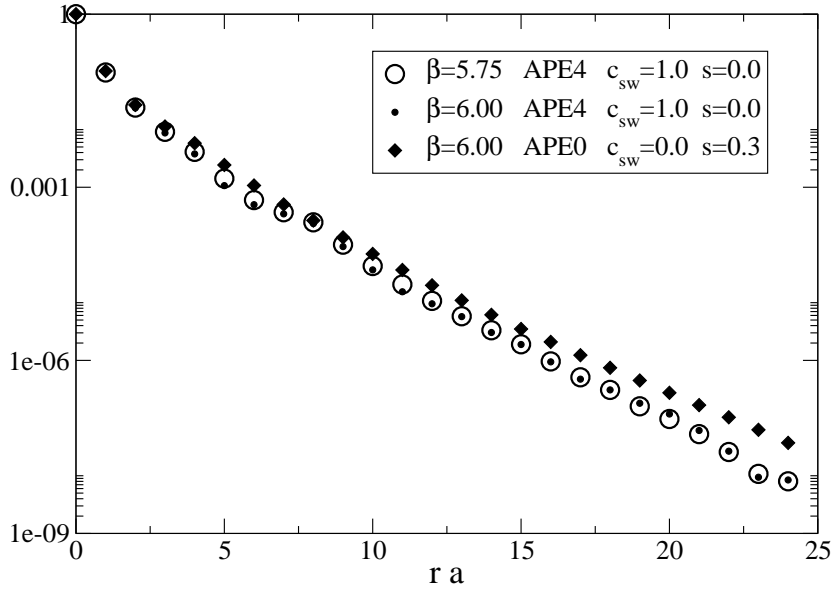


Figure 3: $f(r)$, the maximal matrix element of the overlap as a function of the taxi driver distance r . The small filled and the large empty circles represent the $c_{\text{sw}} = 1$, $s = 0.0$ clover overlap on APE4 gauge backgrounds at $\beta = 5.75$ and $\beta = 6.0$, while the diamonds correspond to the Wilson overlap at the optimal value of $s = 0.3$ on thin link $\beta = 6.0$ gauge backgrounds.

The situation with the FCO action is much simpler. Even after 2-4 steps of APE smearing the gauge field is smooth enough that s can be safely set to the continuum value, zero, regardless of the gauge coupling (at least as long as the quenched Wilson $\beta \geq 5.70$). In Fig. 3 we compare the function $f(r)$ on three 12^4 quenched gauge ensembles. The first two were generated at (Wilson) $\beta = 5.75$ and one with $\beta = 6.00$. The kernel used for the overlap here was the clover action with the perturbative value of $c_{\text{sw}} = 1.0$ and the gauge links have been 4 times APE smeared with $c = 0.45$ (APE4). The two data sets lie so close to each other that they are hardly distinguishable by the naked eye. We also verified that $f(r)$ is the same on two other gauge ensembles with intermediate β values. This means that a 40% decrease in the lattice spacing resulted in no discernible change of the localisation of the overlap; asymptotically it decays as $e^{-\nu r}$ with the same exponent, $\nu = 0.60$. For comparison we also included in the same figure the conventional Wilson overlap on unsmeared $\beta = 6.0$ gauge backgrounds. Here the parameter s was chosen to be 0.3 which is roughly the optimal value for localisation and an exponential fit yielded $\nu = 0.51$ ³

Although the FCO appears to be somewhat more local than the Wilson overlap, the main point here is not this, but that in the case of the former, the range of the operator (in lattice units) can be seen to be independent of the lattice spacing. This strongly suggests that even on gauge backgrounds generated with the Wilson action the FCO stays local in the continuum limit.

To appreciate this statement, let us recall what is known about the locality of the overlap. In Ref. [9] it was shown that it is sufficient for its exponential localisation if the spectrum of $A^\dagger A$ has a gap at zero. It was also suggested there that a finite gap might not be necessary, it might be enough if the continuous spectrum of $A^\dagger A$ is separated from zero. On the other hand, the spectrum is guaranteed to have a finite gap if the gauge field action restricts the plaquette values sufficiently close to unity everywhere. This condition, however, even in the continuum limit, is not necessarily satisfied for practically useful actions.

Although most practical gauge actions damp plaquette fluctuations exponentially in the gauge coupling, the number of plaquettes in a fixed physical volume also grows exponentially in the continuum limit. How the probability of a given plaquette fluctuation in a fixed physical volume will behave in the continuum limit, will depend on which of the two exponentials wins. The results of Ref. [9] therefore do not exclude the possibility that the overlap in gauge backgrounds generated with e.g. the Wilson action becomes non-local in the continuum limit. Even though locality can be proved for special gauge actions, universality cannot be used to argue that any other gauge action in the same universality class will also have the same property. This is because in principle, with a different gauge action, the overlap can be non-local and universality of the complete fermion gauge system is not guaranteed then.

³As in Ref. [9], the fit was done for the range $13 \leq ra \leq 24$ to facilitate the comparison of the exponents ν . We have to note, however that due to finite size effects, the obtained values do not coincide with the asymptotic exponent ν . Nevertheless, they are accurate enough to assess the qualitative differences between various fermion actions.

β	size	a (fm)	V (fm ⁴)	confs	$\rho(0)$ (fm ⁻⁴)
5.745	8 ⁴	0.153	2.27	2000	1.55(1)
5.85	10 ⁴ , 12 ⁴	0.123	2.29, 4.75	3000, 1000	0.78(2)
5.94	12 ⁴	0.104	2.38	1000	0.42(2)

Table 1: The four gauge field ensembles used for the study of the spectrum of $A^\dagger A$ and $(A^\dagger A)^{1/2}$. The lattice spacing has been set with the Sommer parameter $r_0 = 0.49$ fm and the Wilson gauge couplings were tuned to keep the physical volume of the system fixed. The last column lists the spectral density of $(A^\dagger A)^{1/2}$ at zero.

Fortunately the situation is much better since neither the constraint on the plaquette fluctuations nor the one on the spectral gap of $A^\dagger A$ has been proved to be necessary for locality. In fact, based on earlier work of the SCRI group [12], the continuous spectrum of $A^\dagger A$ can be expected to extend all the way down to zero and diverge there as $\lambda^{-1/2}$ at any finite (Wilson gauge action) β . This is because in [12] the spectral density at zero of the Hermitian Wilson Dirac operator,

$$H = \gamma_5(D - 1 - s), \quad (4)$$

was found to be non-vanishing (but exponentially decreasing as a function of β). Using $A^\dagger A = H^2$, the claimed behaviour of spectrum of $A^\dagger A$ immediately follows.

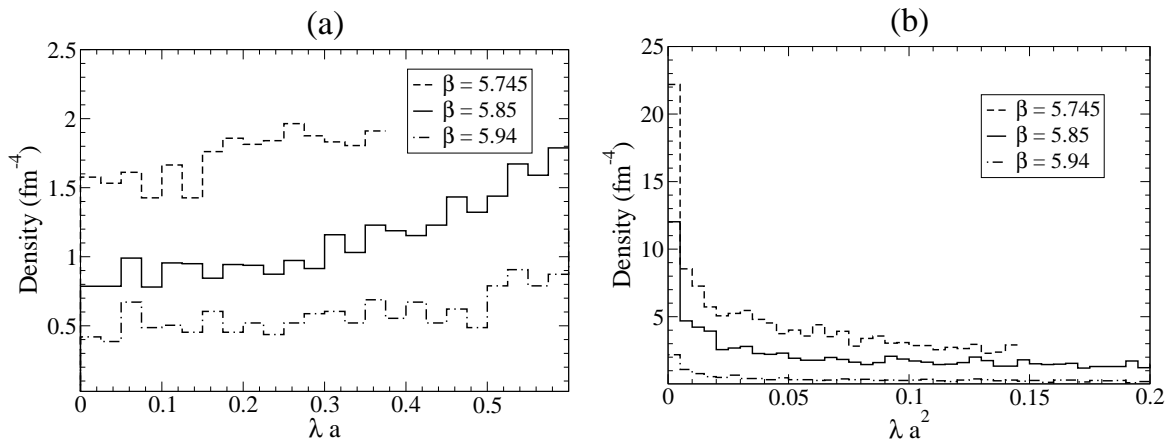


Figure 4: The spectral density of $(A^\dagger A)^{1/2}$ (a), and of $A^\dagger A$ (b), on the APE10 gauge backgrounds of the three fixed physical volume ensembles of Table 1.

We verified this behaviour for the spectrum of the clover $A^\dagger A$ on APE10 quenched gauge backgrounds. In Fig. 4 we plotted the numerically obtained spectral density of both of $(A^\dagger A)^{1/2}$ (a), and of $A^\dagger A$ (b) on the three fixed physical volume gauge ensembles

listed in Table 1. The spectral density of $(A^\dagger A)^{1/2}$ at zero appears to be non-vanishing (Fig. 4a), and the expected singularity of the spectral density of $A^\dagger A$ shows up as a spike at zero (Fig. 4b). We also verified that this qualitative behaviour persists if less or no smearing is applied to the gauge field and the clover term is switched off. In the latter case, however, the numerical value of the spectral density of $(A^\dagger A)^{1/2}$ is almost an order of magnitude higher.

The spectral density of $(A^\dagger A)^{1/2}$ at zero can be quite accurately determined as the slope of a linear fit to the integrated spectral density

$$I(\lambda a) = \int_0^{\lambda a} \rho(x) dx \quad (5)$$

for small values of λ . The obtained values are listed in the last column of Table 1⁴. Although the β range is a bit narrow, this behaviour is consistent with an exponentially falling spectral density that has been already reported for the thin link Wilson operator over a much wider β range [12]. Since our volumes are not particularly big, we also checked that the spectral density obtained on the one available larger volume is consistent with that in the corresponding smaller volume at the same coupling.

Given the fact that even on these locally very smooth smeared gauge fields, on which the average plaquette is at least 2.97, a nonzero spectral density of $(A^\dagger A)^{1/2}$ persists, it is very unlikely that this picture will qualitatively change with any reasonable gauge action or fermion kernel in the overlap. (Of course the numerical value of the spectral density can strongly depend on these details.) The good news is, however that the spectral density decreases with the gauge coupling and as Fig. 3 shows, even at moderately large couplings, these small modes do not seem to have an important impact on the locality of the overlap.

To understand at least qualitatively why this is so, we can look at the localisation of the small eigenmodes of $A^\dagger A$. In Fig. 5 we plotted the participation ratio distribution of low modes of $A^\dagger A$ for the four ensembles listed in Table 1. The participation ratio is defined as

$$P = \frac{\sum_i [\psi(i)^\dagger \psi(i)]^4}{(\sum_i [\psi(i)^\dagger \psi(i)]^2)^2}, \quad (6)$$

where ψ is the wave function and the summation is over the whole lattice. P is a measure of the extension of the wave function; it can vary between $1/V$ (if $\psi^\dagger \psi$ is homogeneously distributed over the whole volume) and 1 (if it is localized on a single site). The important points that can be inferred from Fig. 5 are that small modes of $A^\dagger A$ are rather localized and their localisation (in lattice units) appears to be independent of β as well as of the physical volume. This suggests that these eigenmodes correspond to independent gauge defects that have a fixed size of the order of the cut-off. Moreover, as we have seen, their physical density is decreasing at weaker coupling, therefore they are incapable of propagating quarks to large distances and are very likely to be harmless lattice artifacts that do not influence the locality of the overlap in the continuum limit.

⁴Notice that the spectral density was defined as the number of eigenvalues per fm^4 in terms of the dimensionless eigenvalues λa , therefore its unit is fm^{-4} .

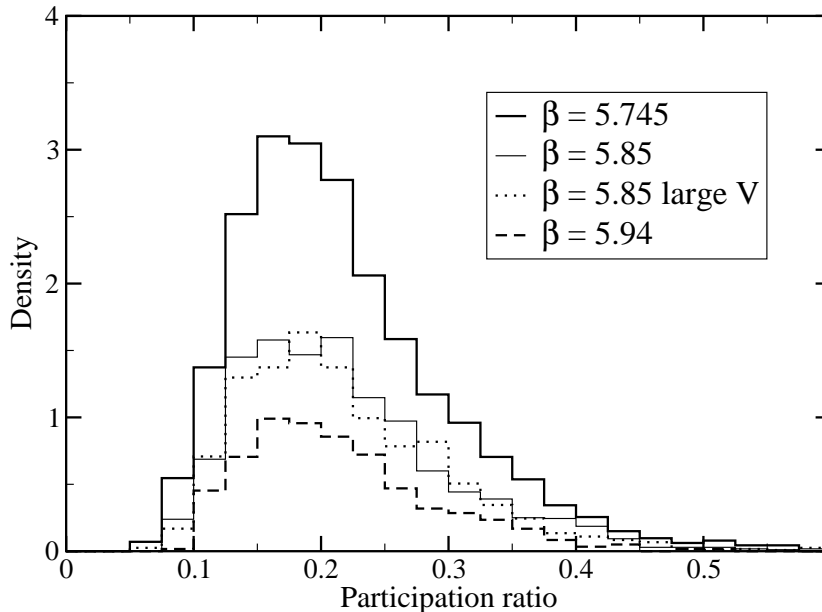


Figure 5: The distribution of participation ratios of low modes ($\lambda_a \leq 0.1$) of the APE10 FCO $A^\dagger A$ on the four gauge ensembles listed in Table 1.

Apart from these theoretical considerations, there is also a practical reason to prefer the FCO action to the WO. We found that, depending on the extent and type of smearing used, the computation of the FCO is a factor 2-5 cheaper than that of the WO. The reason for this is that smearing considerably raises the point where the spectrum of $A^\dagger A$ becomes dense. In our simulation we projected out the 8 lowest eigenmodes of $A^\dagger A$, treated them exactly and approximated the inverse square root of the remainder with Chebyshev polynomials. The degree of the polynomial needed for a given precision is proportional to $\lambda_8^{-1/2}$, where λ_8 is the 8th smallest eigenvalue of $A^\dagger A$. We compared $\langle \lambda_8 \rangle$ for different types of smearing on the $\beta = 5.94$ ensemble of Table 1. As a reference we used the same quantity for the WO (no smearing, $c_{sw} = 0.0$) at $s = 0.4$. The factors of reduction in computation time were the following: 2.2 for APE2, 3.3 for APE4, 4.7 for APE10, all with a smearing factor $c = 0.45$. We also compared these to one level of so called ‘‘HYP’’ smearing, a slightly more complicated smearing that stays within a hypercube [13]. Here we found an improvement factor of 3.7 compared to the WO. Also in other respects (locality of the overlap, density of small modes of $(A^\dagger A)^{-1/2}$) HYP smearing seems to have similar or slightly better properties than APE4 smearing, but it is strictly localized within a hypercube. In this respect HYP smearing probably represents the optimal choice so far for building a FCO action.

3 Topology

3.1 Zero mode wave functions

It has been observed that Wilson overlap quark zero mode wave functions corresponding to smooth instantons are considerably more extended than their continuum counterparts [10]. While this effect is expected to decrease for larger instantons, it can still be important in current lattice simulations where typical instantons are on the scale of a few lattice spacings.

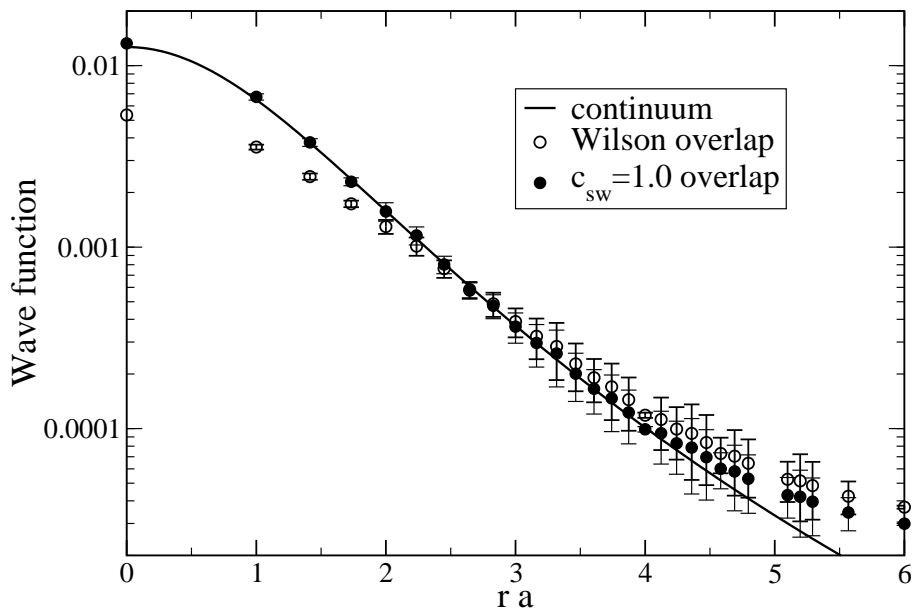


Figure 6: The zero mode wave function $\psi^\dagger\psi(x)$ as a function of the distance from the centre of a size $\rho/a = 2.0$ instanton. Filled symbols represent the $c_{sw} = 1.0$ clover overlap, open symbols correspond to the Wilson overlap and the continuous line shows the analytical continuum expression.

To see how our FCO action fares in this respect, we compared the FCO, the WO and the exact analytical continuum zero mode wave function on discretised lattice instantons of various sizes. Since the instanton backgrounds were locally smooth, we did not apply any smearing in this study, that would not have changed our results appreciably. Both for the FCO and the WO operator time antiperiodic and space periodic boundary conditions were chosen.

Fig. 6 shows a typical result for an instanton size of $\rho/a = 2.0$. The values of $\psi^\dagger\psi(x)$ have been averaged over all the lattice points at a distance $|x| = r$ from the centre of the instanton. Error bars represent the standard deviation of $\psi^\dagger\psi(x)$ at a given distance from the centre. It is non-zero partly because the lattice instanton

was constructed a bit off-site and also because different directions are not equivalent; spherical symmetry is broken by the hypercubic geometry of the finite box.

We can confirm that the WO zero modes are much more extended than the continuum zero modes, as claimed in Ref. [10]. On the other hand the FCO zero modes follow very closely the continuum wave functions even for instanton sizes as small as $a \leq \rho \leq 2a$.

3.2 Index theorem

The Atiyah-Singer index theorem relates the topological charge Q of a smooth continuum gauge field to the number of zero modes of the Dirac operator as

$$Q = N_- - N_+, \quad (7)$$

where N_+ and N_- are the number of positive and negative chirality zero modes [14]. Since the overlap has exact chiral zero modes, it is interesting to ask whether their number with a certain gauge field definition of the charge will satisfy the index theorem.

For the gauge field definition of Q we use the ‘‘Boulder charge’’ which is constructed from two loops in two representations evaluated on smeared gauge links. Details of the construction and its motivation can be found in Ref. [15]. The smearing we chose to use here was 8 steps of APE smearing with $c = 0.45$.

At any finite gauge coupling an exact index theorem cannot be expected to hold. The best one can hope for is that the index theorem be more and more precisely satisfied as the continuum limit is approached. The reason for this is that small topological objects on the scale of the cut-off can occur with a finite probability. Whether a given charge operator will identify such an object or not, can depend on the non-universal details of the operator in question.

It might be possible to detect the occurrence of such an object both with the gauge field charge and the Dirac operator. A topological object on the cut-off scale corresponds to a configuration close to the boundary between two charge sectors. Since the gauge field charge is a continuous function of the field, such an object should be signalled by a gauge field charge that is not close to any integer value. In terms of the overlap, transitions between different topological sectors are singular points. On the other hand, the operator $A^\dagger A$ depends continuously on the gauge field and it has a zero eigenvalue whenever the number of zero modes of the overlap change. Therefore, if the gauge field is in the vicinity of a transition between two charge sectors, it is signalled by a small eigenvalue of $A^\dagger A$.

Based on this intuitive picture, we shall loosely say that a small topological object is detected by a certain charge definition if according to that charge definition the gauge field is ‘‘close’’ to the boundary between different charge sectors. Two topological charge definitions, be they gauge field or fermionic, can be consistent in the continuum limit only if they have the following two properties.

- (A) The density, per unit physical volume, of small, ambiguous topological objects must go to zero in the continuum limit for both definitions of the charge.

(B) If neither charge operator detects a small topological object, they have to give the same charge value.

β	size	a (fm)	$a^2\lambda_{\min} \leq 0.5$	$a^2\lambda_{\min} \leq 0.2$	$\Delta Q \geq 0.1$	$\Delta Q \geq 0.2$
5.745	8^4	0.153	0.97	0.824	n.a.	n.a.
5.85	10^4	0.123	0.863	0.637	0.652	0.457
5.94	12^4	0.104	0.676	0.431	0.497	0.335
6.033	14^4	0.088	0.456	0.243	0.335	0.210

Table 2: The fraction of configurations “close” to the boundary between charge sectors, according to different criteria. λ_{\min} is the smallest eigenvalue of $A^\dagger A$, ΔQ is the distance of the Boulder charge Q from the nearest integer. (Q was not computed on the coarsest ensemble.)

At first sight property (A) might seem trivially true, but in fact there are examples when it does not hold. This is the case e.g. in quenched SU(2) gauge theory with the Wilson action and the geometric charge. The dislocation problem [16], appearing there, is essentially equivalent to the violation of property (A). Whether (A) is satisfied in a particular case, depends both on the action and the charge operator.

In Table 2 we demonstrate how the probability of configurations with an “ill defined” charge changes with β . For the fermionic definition, we listed the fraction of configurations on which the smallest eigenvalue of $A^\dagger A$ was below 0.5 (0.2). For the gauge field definition we computed the fraction of configurations with a charge farther than 0.2 (0.1) from the nearest integer. According to all these criteria the charge appears to become more well-defined for weaker coupling. We emphasize that throughout this study the number of smearing steps was kept fixed at 10 (and 8) for the fermionic (and the gauge) definition of the charge.

It was also essential to keep the physical volume of the compared configurations constant as β was increased. If our intuitive picture is correct, and the boundary between charge sectors is associated with localized small defects, we expect that in larger volumes the charge becomes ill defined more frequently (at fixed β).

Let us see whether our gauge and fermionic charge definition satisfy criterion (B). In Fig. 7 we show a scatter plot of the difference between the fermionic and the gauge field charge versus the smallest eigenvalue of $A^\dagger A$ on 2000 gauge configurations obtained at two values of β on the same physical volume. It is clear that if $a^2\lambda_{\min}$ is larger than about 0.4 – 0.6, the two charge definitions are rather close. This means that (B) is also satisfied.

Interestingly enough, on these locally smooth gauge backgrounds there is a good correlation between small eigenmodes of $A^\dagger A$ and change of topology. We would like to remark that while the latter implies the former by continuity, the argument does not hold the other way round. It is not guaranteed that a small mode of $A^\dagger A$ implies that

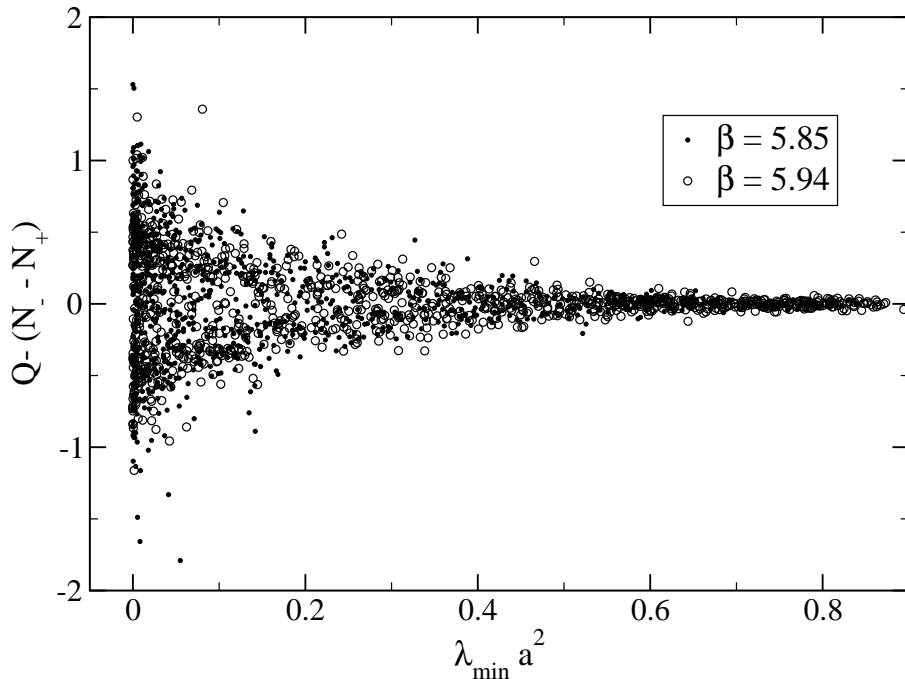


Figure 7: Scatter plot of the difference between the APE10 FCO overlap zero mode charge and the gauge field charge versus the smallest eigenvalue of $A^\dagger A$. Two ensembles of 1000 configurations were plotted from Table 1.

the gauge configuration is close to the boundary between charge sectors. In fact, on unsmearred configurations the density of small modes is much larger and it is possible that many or even most of these small modes are not related to topology.

3.3 Topological susceptibility

We also computed the quenched zero mode susceptibility

$$\chi_{\text{zm}} = \frac{1}{V} \langle (N_+ - N_-)^2 \rangle, \quad (8)$$

with the APE10 FCO action as well as the topological susceptibility

$$\chi_{\text{top}} = \frac{1}{V} \langle Q^2 \rangle, \quad (9)$$

with the APE8 Boulder charge. The results are summarized in Fig. 8. In addition to the ensembles listed in Table 1, here we also used a coarser ensemble of 1000 6^4 lattices with $\beta = 5.62$ and a finer one of 200 14^4 lattices at $\beta = 6.033$. On the two coarsest ensembles the Boulder charge was not computed, while on the finest

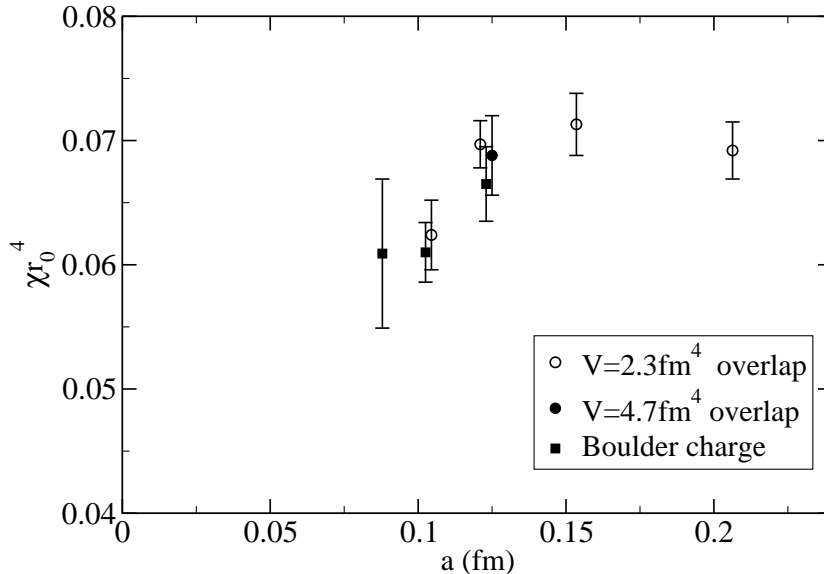


Figure 8: The topological susceptibility as a function of the lattice spacing. The scale was set with the Sommer parameter $r_0 = 0.49$ fm.

one, we computed only the Boulder charge. The physical volumes were chosen to be approximately the same, except for the 12^4 $\beta = 5.85$ ensemble where the volume was about two times bigger to test finite volume effects. Although the fixed volumes $V \approx 2.3 \text{ fm}^4$ are not particularly big, no finite size effects can be observed. After the discussion in the previous subsection, it does not come as a surprise that the Boulder charge susceptibility and the overlap zero mode susceptibility appear to be compatible whenever both are available.

There is no simple trend as to how the susceptibility changes with β , most likely because our β range at weak couplings is rather limited. For this reason we do not attempt a continuum extrapolation. Our results, however, at the weakest two couplings are consistent with those of the other available high statistics chiral fermion computation of the quenched susceptibility [4].

4 Conclusions

In the present paper we studied the properties of fat link clover overlap actions. The motivation came from the already known good properties of fat link clover actions [17]. It turns out that if used in the overlap construction, much less smearing (2-4 steps of APE smearing or 1 step of HYP smearing) is enough to guarantee a substantial improvement in several properties. In particular, we showed here that the localisation range of the FCO action in quenched gauge backgrounds is independent of the gauge

coupling in the range of Wilson $5.75 \leq \beta \leq 6.00$, suggesting that the FCO remains local in the continuum limit.

Another advantage of the construction is that in contrast to the Wilson overlap (WO), the parameter s does not need to be optimized, one can simply use the tree level value $s = 0.0$. The FCO also turns out to be slightly more local than the WO at the optimal value of s . The improvement in this respect, however, is not nearly as significant as in the case of more complicated fermion actions [4, 5, 6]. Smearing also improves the condition number of $A^\dagger A$ and results in a saving of a factor of 2-5 in CPU time when evaluating the overlap. Finally, in contrast to the WO, the FCO action correctly describes fermion zero mode wave functions of instantons as small as the cut-off.

We explicitly studied the locality of the involved smearing. We found that 2-4 steps of APE smearing (with a smearing coefficient of $c = 0.45$) can be safely used; the range of the smearing is bounded with an exponential with an exponent much bigger than 1 (in lattice units). For some purposes, as much as 10 smearing steps might still be acceptable. Probably the best compromise between locality and efficiency is hypercubic smearing that mixes only gauge degrees of freedom within a hypercube [13].

We also studied the connection between small modes of $A^\dagger A$ and the locality of the overlap. Smearing together with the clover term considerably reduces the density of low modes of $A^\dagger A$ but the spectral density still appears to be divergent at zero. This is a simple consequence of the fact that the Hermitian Dirac operator $H = \gamma_5(D - 1)$ has a non-vanishing spectral density at zero. Our results show that small modes of H (or $A^\dagger A$) do not affect the locality of the overlap in practice. The reason for this is that the low modes are typically localized at the scale of the cut-off, their localisation (in lattice units) does not change as the lattice spacing shrinks, but their physical density rapidly decreases at the same time.

Low modes of $A^\dagger A$ can signal that the gauge field configuration is “close” to the boundary between topological sectors, as defined with the corresponding overlap. We also used the Boulder charge (a field theoretic definition) to monitor whether the gauge field is close to a transition between charge sectors. We found that whenever the gauge field is far away from such a transition according to both the fermionic and the gauge field definition, the two charge definitions are always consistent. Moreover, the occurrence of configurations close to the transition region becomes more rare as β increases, while the physical volume stays fixed. This suggests that in the continuum limit the FCO fermionic and Boulder field theoretic charge satisfy the index theorem. In this connection we also discussed the general criteria for two charge definitions to give consistent results in the continuum limit. Finally we also presented a high statistics computation of the quenched topological susceptibility with the fermionic definition involving the FCO action.

Fat link clover overlap actions can represent the optimal compromise between complexity on the one hand and good physical properties and efficiency on the other hand. This might be the case also in future dynamical overlap simulations, especially if hybrid Monte Carlo cannot be implemented with the overlap.

Acknowledgments

I would like to thank the MILC collaboration [18] and the creators of the ARPACK package [19] for making their code publicly available, as well as Anna Hasenfratz for discussions and for providing the code for HYP blocking. This work was supported by the EU's Human Potential Program under contract HPRN-CT-2000-00145, by Hungarian science grant OTKA-T032501, and also partly by a Bolyai Fellowship.

References

- [1] P. Hernandez, Nucl. Phys. Proc. Suppl. **106** (2002) 80 [arXiv:hep-lat/0110218].
- [2] R. Narayanan and H. Neuberger, Phys. Rev. Lett. **71** (1993) 3251 [arXiv:hep-lat/9308011]. Nucl. Phys. B **412**, 574 (1994) [arXiv:hep-lat/9307006]; Nucl. Phys. B **443**, 305 (1995) [arXiv:hep-th/9411108].
- [3] M. Albanese *et al.* [APE Collaboration], Phys. Lett. B **192** (1987) 163.
- [4] P. Hasenfratz, S. Hauswirth, T. Jorg, F. Niedermayer and K. Holland, arXiv:hep-lat/0205010.
- [5] T. DeGrand [MILC collaboration], Phys. Rev. D **63** (2001) 034503 [arXiv:hep-lat/0007046].
- [6] W. Bietenholz, arXiv:hep-lat/0204016.
- [7] T. G. Kovacs, arXiv:hep-lat/0111021.
- [8] W. Kamleh, D. Adams, D. B. Leinweber and A. G. Williams, arXiv:hep-lat/0112041.
- [9] P. Hernandez, K. Jansen and M. Luscher, Nucl. Phys. B **552** (1999) 363 [arXiv:hep-lat/9808010].
- [10] C. Gattringer, M. Gockeler, C. B. Lang, P. E. Rakow and A. Schafer, Phys. Lett. B **522** (2001) 194 [arXiv:hep-lat/0108001].
- [11] I. Horvath, Phys. Rev. Lett. **81** (1998) 4063 [arXiv:hep-lat/9808002]; I. Horvath, C. T. Balwe and R. Mendris, Nucl. Phys. B **599** (2001) 283 [arXiv:hep-lat/0006027].
- [12] R. G. Edwards, U. M. Heller and R. Narayanan, Phys. Rev. D **60** (1999) 034502 [arXiv:hep-lat/9901015].
- [13] A. Hasenfratz and F. Knechtli, Phys. Rev. D **64** (2001) 034504 [arXiv:hep-lat/0103029].

- [14] M. F. Atiyah and I. M. Singer, *Annals Math.* **93** (1971) 139.
- [15] A. Hasenfratz and C. Nieter, *Phys. Lett. B* **439** (1998) 366 [arXiv:hep-lat/9806026]; T. DeGrand, A. Hasenfratz and T. G. Kovacs, *Nucl. Phys. B* **505** (1997) 417 [arXiv:hep-lat/9705009].
- [16] D. J. Pugh and M. Teper, *Phys. Lett. B* **224** (1989) 159. M. Gockeler, A. S. Kronfeld, M. L. Laursen, G. Schierholz and U. J. Wiese, *Phys. Lett. B* **233** (1989) 192.
- [17] T. DeGrand, A. Hasenfratz and T. G. Kovacs, *Nucl. Phys. B* **547** (1999) 259 [arXiv:hep-lat/9810061].
- [18] The MILC code is available at <ftp://ftp.physics.utah.edu/pub/milc/freeHEP/>.
- [19] D.C. Sorensen, *SIAM J. Matrix Analysis and Applications*, **13(1)** (1992) 357; the package is available at <http://www.caam.rice.edu/software/ARPACK/>.